Supplementary of

Impact of biomass burning aerosols on radiation, clouds, and precipitation over the Amazon during the dry season: dependence of aerosol-cloud and aerosol-radiation interactions on aerosol loading

Lixia Liu[1], Yafang Cheng[1], Siwen Wang[1], Chao Wei[1], Mira Pöhlker[1], Christopher Pöhlker[1], Paulo Artaxo[2], Manish Shrivastava[3], Meinrat O. Andreae[1,4], Ulrich Pöschl[1] and Hang Su[1]

[1] Max Planck Institute for Chemistry, Mainz, Germany

[2] Institute of Physics, University of São Paulo, São Paulo 05508-900, Brazil

[3] Pacific Northwest National Laboratory, Richland, Washington, USA

[4] Scripps Institution of Oceanography, University of California at San Diego, La Jolla, California, USA

Correspondence to: *yafang.cheng@mpic.de & h.su@mpic.de*

Table S1. Estimates of radiative perturbation by biomass burning aerosols over the Amazon Basin in this study and from previous studies.

	Description	Radiative perturbation (W m^{-2})*	AOD	Effect	Region of Amazon Basin	Model	Reference
Clear-sky	SW at TOA	–5.6±1.7	0.25±0.11	ARI	Southern	SBDART	Sena et al. (2013)
	SW at TOA	–3.33±0.89	0.67	total	Southern	HadGEM3-GA3	Thornhill et al. (2018)
	SW at TOA	[–0.7, –3.7]	0.2–0.6	ARI	Central	WRF-Chem	This study
All-sky	SW at TOA LW at TOA SW at surface	1.35±1.8 –3.07±1.55 –5.46±1.93	0.67	total	Southern	HadGEM3-GA3	Thornhill et al. (2018)
	SW at TOA	–1.75 2.72 1.53	0.8–1.2 0.4–1.0 0.4–1.0	ARI	Southwest	WRF-Chem	Archer-Nicholls et al. (2016)
	SW+LW at TOA SW+LW at surface	–4±1 –9±1		ARI	Southern	MetUM	Kolusu et al. (2015)
	LW at TOA SW at surface	–0.12 –15.9		total	entire	WRF-Chem	Wu et al. (2011)
	SW at surface LW at surface	–28.23 8.6	0.633	total	Southern	GATOR-GCMOM	Ten Hoeve et al. (2012)
	SW at surface	–10	0.2–0.4	ARI	Northwest	CCATT-BRAMS	Rosario et al. (2013)
	SW at TOA LW at TOA SW at surface LW at surface	[–0.3, 0.6] [0.1, 0.9] [–6.7, –31.8] [0.3, 1.9]	0.2–0.6	total	Central	WRF-Chem	This study
	SW at TOA LW at TOA SW at surface LW at surface	[0.4, 2.0] [0.1, 1.0] [–5.7, –30.5] [0.4, 2.0]	0.2–0.6	ARI	Central	WRF-Chem	This study

*Radiative perturbation with standard deviation or in bracket for range obtained from simulations with emission intensity of EMIS1–EMIS6.

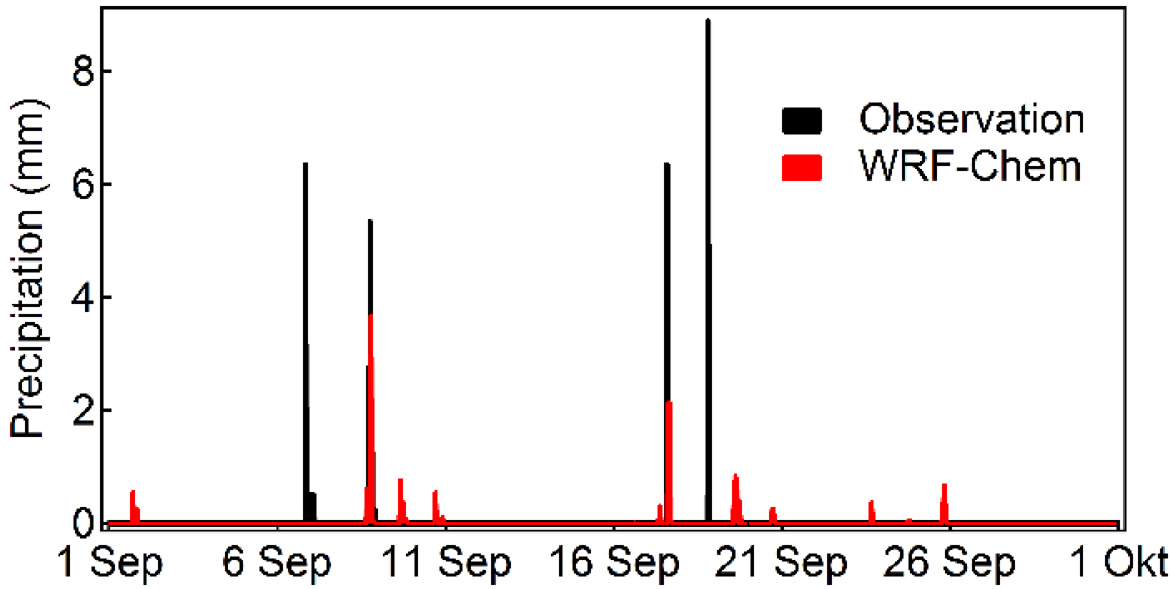

Figure S1. Time series of precipitation from observations at the ATTO site and WRF-Chem simulations during September 2014.

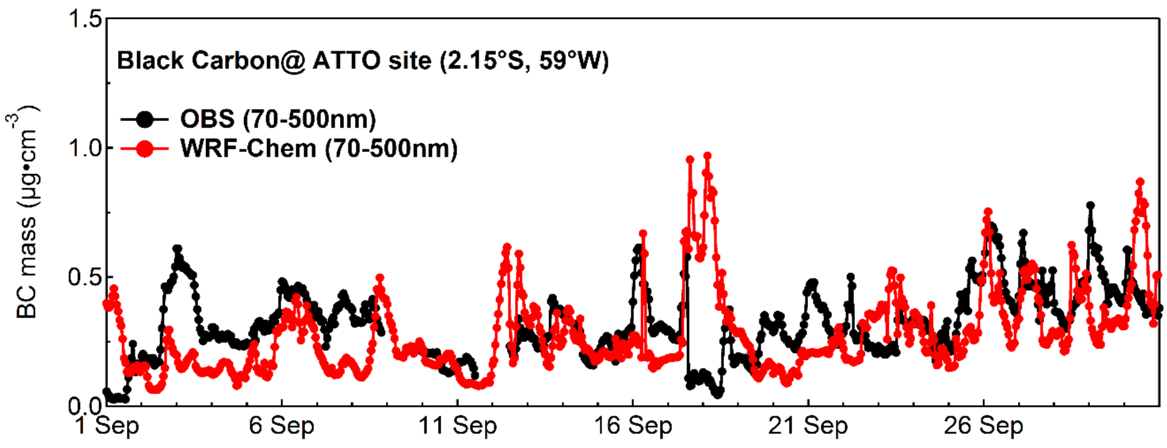

Figure S2. Time series of simulated and observed black carbon mass concentrations at the ATTO site.

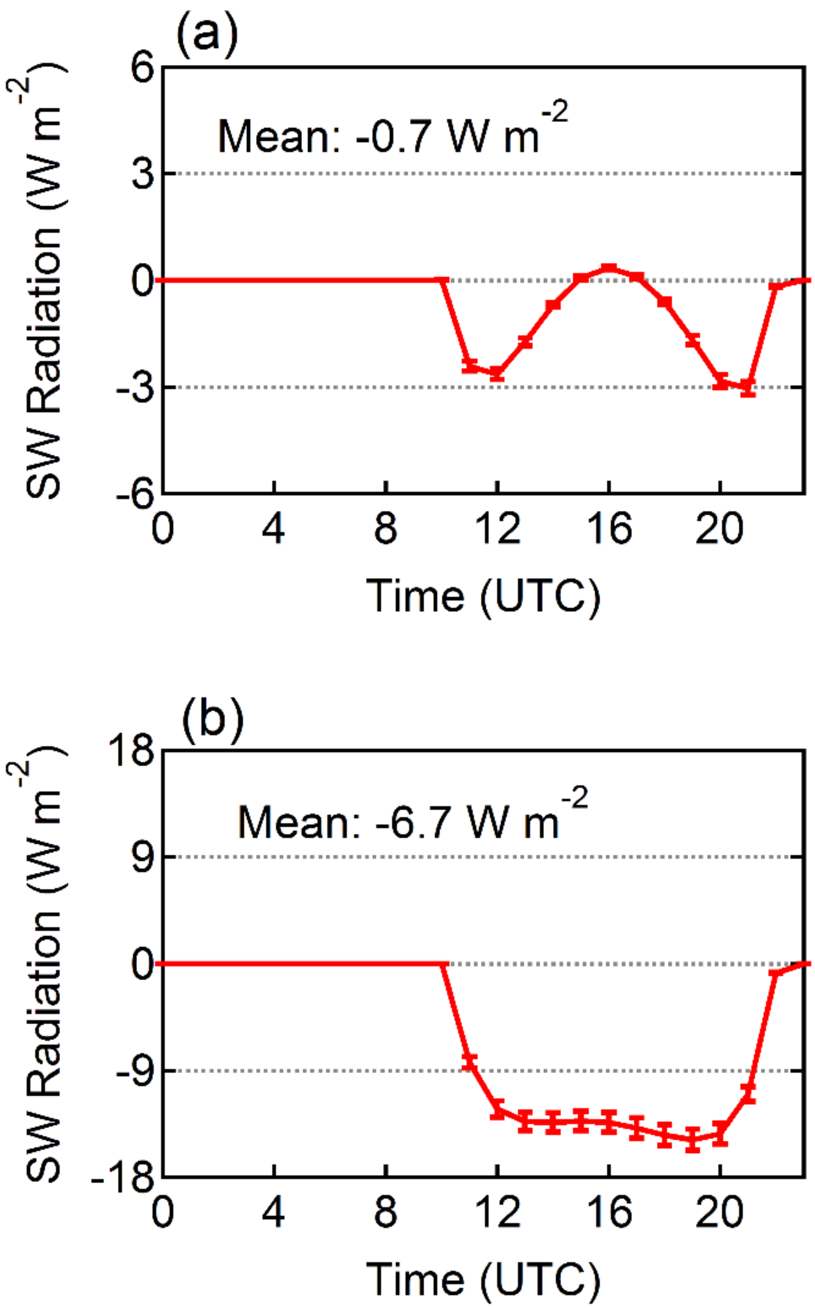

Figure S3. Diurnal variation of changes in clear-sky shortwave radiation at TOA (a) and at the surface (b) due to ARI in the EMIS1 emission scenario. Error bars denote the standard error.

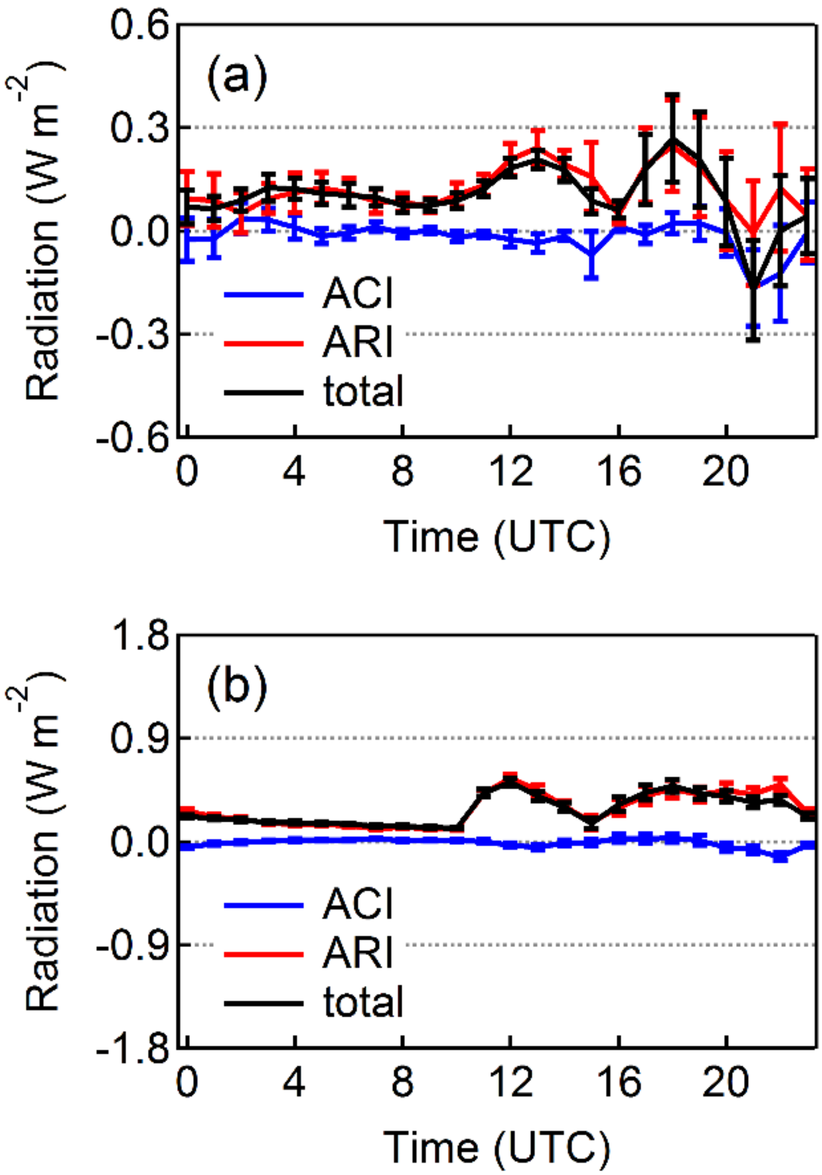

Figure S4. Diurnal variation of changes in all-sky longwave radiation at TOA (a) and at the surface (b) in the EMIS1 emission scenario. Error bars denote the standard error.

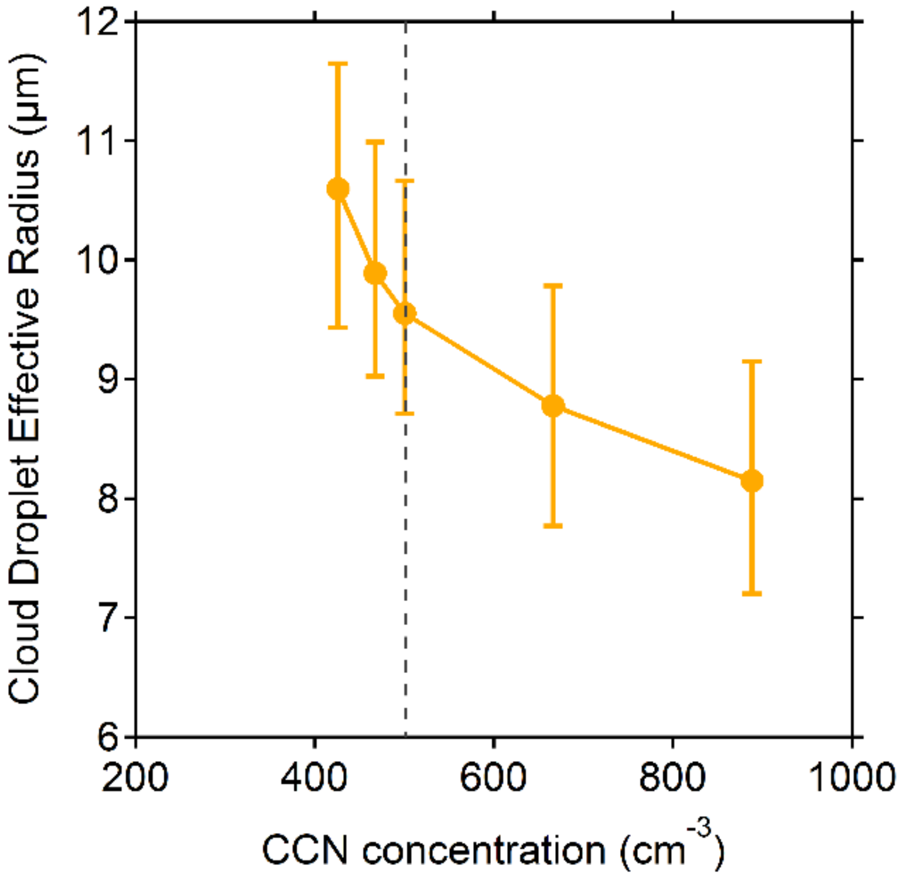

Figure S5. Relationship of monthly mean domain-averaged cloud droplet effective radius and cloud-base CCN concentrations for all emission scenarios derived from experiments of CCNR3 and PCNR3_EMISX. The dashed line indicates the EMIS1 scenario. Error bars represent the 25th and 75th percentiles of all domain-averaged data in each simulation.

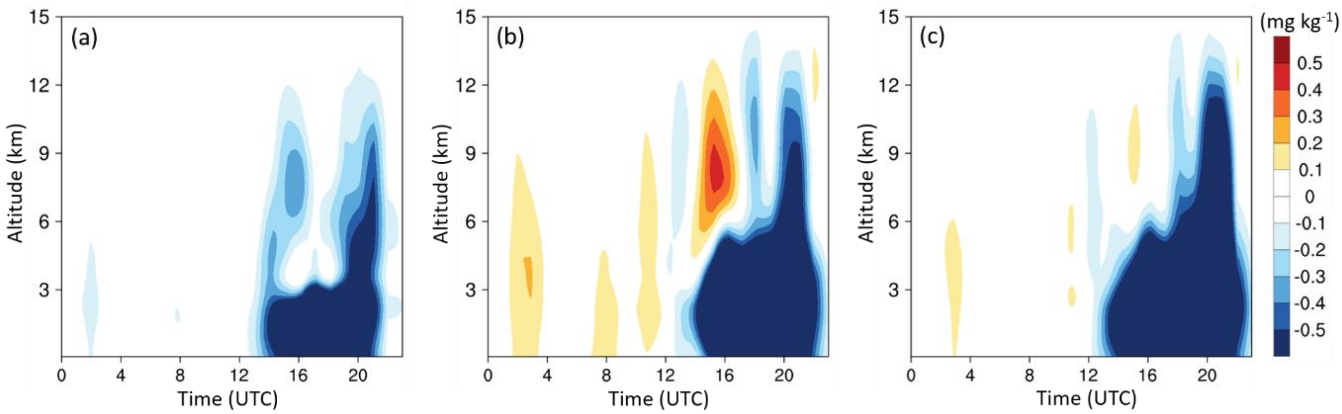

Figure S6. Diurnal variation of the vertical distribution of the domain-averaged difference in precipitating hydrometer (QRAIN+QSNOW+QGRAUP) concentrations caused by BB aerosols' ACI (a), ARI (b), and total effect (c) in the EMIS6 emission scenario.

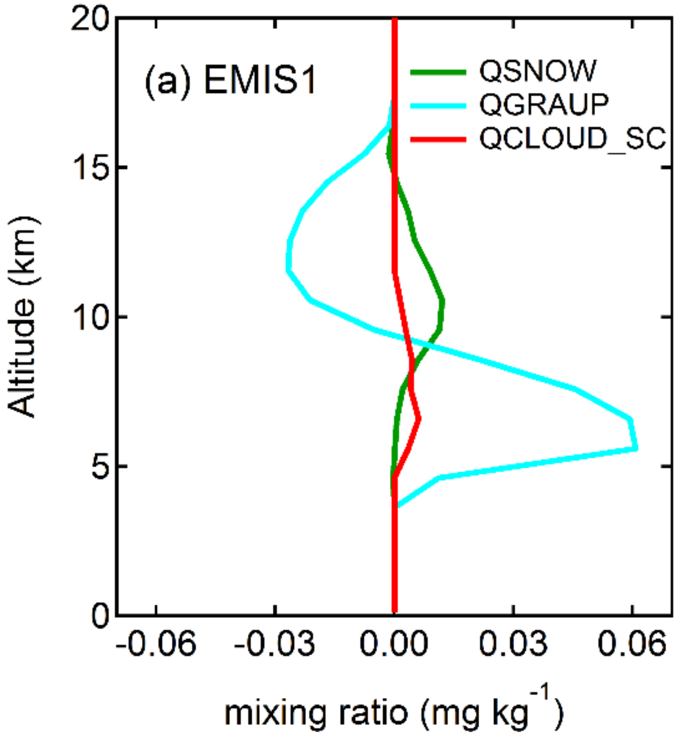

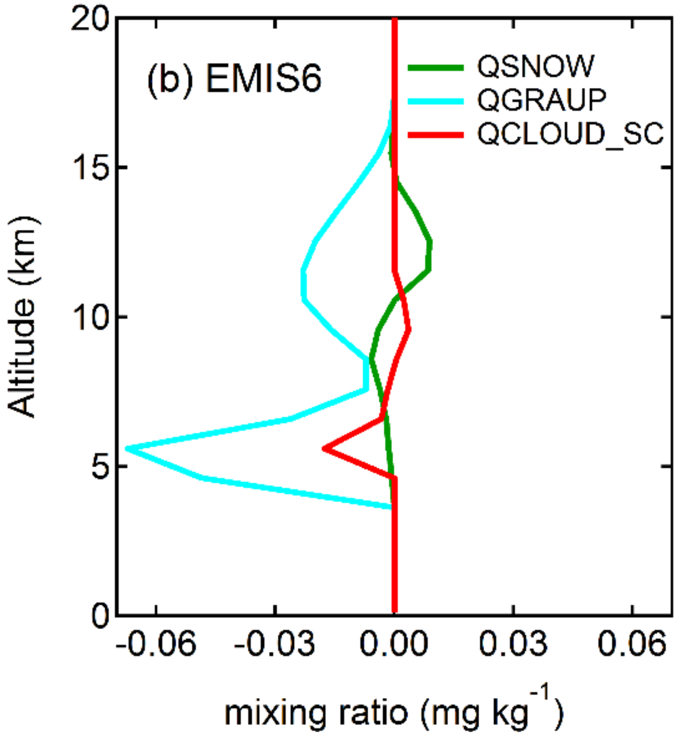

Figure S7. Profiles of ARI-induced changes in snow, graupel, and super-cooled cloud water mixing ratios for emission scenarios EMIS1 (a) and EMIS6 (b).

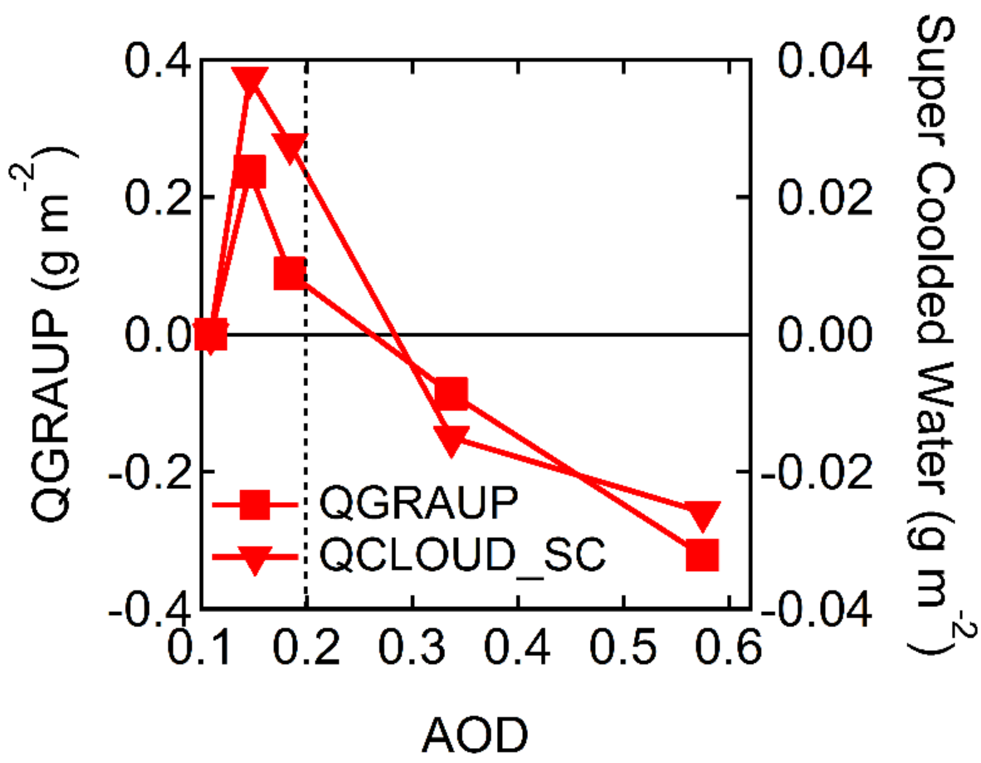

Figure S8. ARI-induced changes in column-integrated graupel and super-cooled cloud water content with increasing BB emission intensity (indicated by the domain-averaged AOD in each emission scenario). The vertical dotted line in each plot indicates the EMIS1 scenario.